Polymorphs and Hydrates of Acyclovir

KATIE M. LUTKER, ROSALYNN QUIÑONES, JIADI XU, AYYALUSAMY RAMAMOORTHY, ADAM J. MATZGER

Department of Chemistry, Biophysics, and the Macromolecular Science and Engineering Program, The University of Michigan, 930 North University, Ann Arbor, Michigan 48109-1055

ABSTRACT: Acyclovir (ACV) has been commonly used as an antiviral for decades. Although the crystal structure of the commercial form, a 3:2 ACV/water solvate, has been known since 1980s, investigation into the structure of anhydrous ACV has been limited. Here, we report the characterization of four anhydrous forms of ACV and a new hydrate in addition to the known hydrate. Two of the anhydrous forms appear as small needles and are stable to air exposure, whereas the third form is morphologically similar but quickly absorbs water from the atmosphere and converts back to the commercial form. The high-temperature modification is achieved by heating anhydrous form I above 180°C. The crystal structures of anhydrous form I and a novel hydrate are reported for the first time. © 2010 Wiley-Liss, Inc. and the American Pharmacists Association J Pharm Sci 100:949–963, 2011

Keywords: polymorphism; hydrates; X-ray diffractometry; Raman spectroscopy; crystal structure; calorimetry (DSC); solid-state NMR spectroscopy; FTIR spectroscopy

INTRODUCTION

Solid form diversity in organic compounds is a widespread phenomenon that encompasses crystal polymorphism, solvates, and cocrystals; in the case of active pharmaceutical ingredients, the different physical properties that forms display can influence properties including bioavailability and morphology, among others.[1] Conformational flexibility and hydrogen bonding are considered factors that influence the ability of a molecule to form polymorphs,[2] but these are not the only contributing factors and, in some cases, are completely absent. Polymorphism is traditionally investigated through the use of different solvents and temperatures of crystallization, whereas newer methods for the discovery and control of solid forms include polymer-induced heteronucleation (PIHn).[3,4] Here, the crystallization of acyclovir (ACV, Fig. 1) is reported using PIHn and traditional solid form discovery techniques. The ability of ACV to exist in multiple hydrogen bonding networks and its flexible side chain are important factors to be considered when investigating the existence of and characterizing the multiple solid forms of this drug. Crystal forms were characterized by Raman spectroscopy,

powder X-ray diffraction (PXRD), single crystal X-ray diffraction, differential scanning calorimetry (DSC), Fourier transform infrared (FTIR) spectroscopy, solid-state nuclear magnetic resonance (SS-NMR) spectroscopy, and thermogravimetric analysis (TGA).

Acyclovir is a guanine derivative possessing antiviral activity and commonly used in the treatment of herpes. Previous studies have yielded the crystal structure of the commercial form, a 3:2 ACV/water hydrate.[5,6] This hydrate crystallizes in the monoclinic space group $P2_1/n$ with cell parameters of $a = 25.459(1)$ Å, $b = 11.282(1)$ Å, $c = 10.768(1)$ Å, and $\beta = 95.16(1)°$ (Fig. 2).[6] A previous study by Kristl et al.[7] proposed the existence of two stable anhydrous forms and an unstable form but provided characterization limited to thermal analysis and dissolution rates of the forms. Recently, Sohn and Kim[8] showed the existence of two anhydrous polymorphs in addition to the known hydrate and an acetic acid solvate through PXRD, thermal analysis, and dissolution rates. The packing arrangement of the anhydrous form versus that of the commercial hydrate remains unknown and is of particular interest due to previous findings that the hydrate has a faster dissolution rate than the anhydrous form[7]; this observation contrasts with the trend typically observed in the literature where anhydrous forms dissolve more quickly than the hydrate.[7,9] Here, we demonstrate that ACV displays, at minimum, two anhydrous forms stable
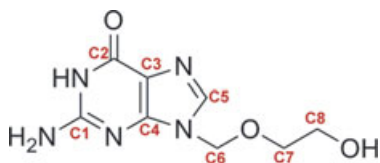
Figure 1. Molecular structure of acyclovir (also known as 2-amino-9-((2-hydroxyethoxy)methyl)-1H-purin-6(9H)-one).

under ambient conditions, two forms that do not exist under ambient conditions, and two hydrates. In addition, structure determination by single crystal X-ray diffraction was carried out to better understand the molecular packing arrangements and properties of each form of ACV.

Experimental

Materials

Commercial ACV (Spectrum, Gardena, California) was used as supplied. Solvents, purchased from Fisher Scientific (Fairlawn, New Jersey), were used directly.

Preparation of Polymorphs and Hydrates

Form I of ACV was obtained by heating a sample of commercial ACV at a rate of 5°C/min to 180°C on a hotstage and then allowing the sample to cool. Single crystals of form I were obtained during polymorph screening using polymeric heteronuclei by crystallizing from a methanol solution in the presence of Nylon 6. Form II was obtained by heating 20.0 mg of commercial ACV in 20 mL of methanol to 68°C in a closed vessel until complete dissolution was achieved and then allowing the solution to evaporate quickly while heat was still being applied. Single crystals of form II were obtained from evaporating a methanol solution of ACV in the presence of Nylon 6/12. Form III is a metastable form that is obtained by heating commercial ACV (denoted here as form V) on a hotstage to a temperature between 130°C and 150°C. Form IV is a high-temperature modified form that is formed by heating form I above 180°C. Form VI, a 1:2 ACV/H$_2$O hydrate, was found during a polymorph screening using polymeric heteronuclei and was found to crystallize in the presence of poly(ethylene terephthalate), poly(vinyl chloride), poly(vinyl stearate), and polypropylene. Nylon 6/12 yielded a mixture of forms II and VI. Single crystals of appropriate size and quality of form VI were obtained on a terpolymer derived from 29% (ethoxyethyl)methacrylate, 38% methylmethacrylate, and 33% divinyl benzene. Form V, the commercial 3:2 ACV/H$_2$O hydrate, was used as supplied.

Raman Spectroscopy

Raman spectra were recorded on a Renishaw inVia Raman microscope equipped with a 20× objective and utilizing a 633-nm laser. The scan range was 100 to 3600 cm^{-1}, using three scans of 30-s length each per spectrum. Samples were analyzed on an aluminum foil holder and a silicon standard was used to calibrate the instrument. Variable temperature Raman spectroscopy was performed using a Linkam LTS 350 hotstage equipped with a TMS 94 controller. Samples were analyzed using a 647-nm laser over a scan range of 100 to 3600 cm^{-1}. The heating rate was controlled using Renishaw Wire 2.0 software.

Infrared Spectroscopy

Fourier transform infrared spectroscopy analyses were performed on forms I, II, and V using an attenuated total reflectance accessory (ATR; ThermoNicolet Avatar model 360-FTIR). The scan range was 700 to 3800 cm^{-1}, employing 1024 scans with a resolution of 1 cm^{-1}. Samples were analyzed on the ATR stage and the empty stage was used as the background.

X-ray Diffraction

Powder X-ray diffraction patterns were obtained on a Rigaku R-Axis Spider diffractometer at 50 kV and 40 mA, using monochromated Cu Kα radiation (1.5406 Å). Samples were packed in a glass capillary and run at room temperature. Images were integrated from 2.5° to 50° 2θ using the AreaMax^2 software package and the resulting pattern was analyzed using MDI Jade 8. Variable temperature PXRD was performed by heating the sample in a glass capillary at 1°C/min, using an Oxford Cryostream Plus instrument. The unit cell constants of form II were determined on this instrument at 90 K by indexing several crystals in single crystal mode; however, none of these were judged suitable for structure determination.

Crystal structures were obtained on a Bruker SMART CCD-based X-ray diffractometer equipped with an LT-2 low-temperature device and normal focus Mo-target X-ray tube ($\lambda = 0.71073$) operated at 2000-W power (50 kV, 40 mA). The X-ray intensities were measured at 85 (2) K; the detector was placed at a distance 4.980 cm from the crystal. Analysis of the data showed negligible decay during the data collection; the data were processed with SADABS and corrected for absorption. Structures were solved and refined with the Bruker SHELXTL (version 6.12) software package. All nonhydrogen atoms were refined anisotropically, with the hydrogen atoms placed in idealized positions.

Thermomicroscopy

A Mettler Toledo FP82HT hotstage with a FP 90 control processor was used for thermomicroscopy. The

sample was observed under polarized light with a Leica DMLP microscope. Initially, samples were heated from 30°C to 250°C at a rate of 5°C/min. The transformation product was then identified using Raman spectroscopy and/or PXRD. The hotstage was calibrated using a caffeine standard.

Differential Scanning Calorimetry

Differential scanning calorimetry was performed on a TA Instruments DSC Q10 calorimeter. Samples were placed in hermetic aluminum pans and sealed using a TA crimper. The temperature range was 25°C to 300°C, with a heating rate of 10°C/min. The calorimeter was calibrated using an indium standard.

Thermogravimetric Analysis

Thermogravimetric analysis was performed on a TA Instruments Q50 TGA thermogravimetric analyzer. Samples were heated at a rate of 20°C/min from room temperature to 600°C. Calibration of the instrument was performed using nickel and alumel standards.

Solid-State ^{13}C Nuclear Magnetic Resonance

^{13}C solid-state NMR spectra of forms I and II were obtained on a Varian VNMR J 600 MHz NMR system equipped with a 4-mm double-resonance magic angle spinning (MAS) probe using a Ramp-CP cross-polarization technique.[10] Other experimental parameters include contact time of 2-ms CP time, recycle delay of 3 s, spinning speed of 18 kHz, and 80-kHz TPPM (two-phase pulse modulation) proton-decoupling during acquisition.[11]

Calculations of ^{13}C chemical shifts were carried out using the gauge-including atomic orbitals (GIAO) method in the Gaussian03 program and the B3LYP hybrid functional.[12] Several basis sets ranging from 6-31G to 6-311++G (2d,p) were used to determine the effect of the basis set size on predicted chemical shift. Geometries for calculations were obtained by optimizing hydrogen atoms positions determined by crystallography (B3LYP /6-31G*) while freezing the heavy atom positions.[13]

RESULTS AND DISCUSSION

The relationships among the forms of ACV are discussed in the following text in the context of each of the analytical method employed. Figure 2 summarizes the conditions under which transformations occur between forms.

Raman Spectroscopy

Raman spectroscopy is a reliable way to differentiate among ACV forms. The most distinctive region is between 600 and 700 cm^{-1}. In this region, form I has two peaks at 641.5 and 670.4 cm^{-1} with a small peak at 688.5 cm^{-1}, whereas form II has four peaks in the region at 632.5, 638.2, 666.2, and 686.8 cm^{-1} with a small peak at 700.8 cm^{-1}. Form III has three peaks at 639.3, 658.9, and 672.8 cm^{-1}. The new hydrate, form VI, has three peaks at 640.1, 659.7, and 685.1 cm^{-1}, whereas form V, the commercially available hydrate, has five peaks at 634.1, 644.0, 658.0, 681.9, and 698.4 cm^{-1}. In the carbonyl and C—N region, the forms also differ, probably due in part to differences in the hydrogen bonding motifs. Form I has peaks at 1606.3, 1628.5, and 1675.5 cm^{-1}, whereas form II has peaks at 1645.8 and 1702.7 cm^{-1}. Form III has peaks at 1614.2, 1630.6, 1672.3, and 1692.0 cm^{-1}. The hydrates also differ in this region with form VI having peaks at 1625.7, 1631.4, and 1701.8 cm^{-1} and form V also having three peaks at 1614.5, 1631.8, and 1695.3 cm^{-1}. Other distinctive regions in the spectra are between 100–200 and 1500–1600 cm^{-1}. The Raman spectrum of the high-temperature modification, form IV, was found to be very similar to that of form I with the exception of the peak at 1482 cm^{-1}, which is shifted discontinuously at the phase transition temperature to 1480 cm^{-1}. The Raman spectra are shown in Figure 3. (Table 1 contains a listing of peaks.)

Variable temperature Raman spectroscopy shows the progression of transformations occurring during the heating of the hydrate form V (Fig. 4). The plot shows a transition from form V to form III, to form I, and then to form IV. Dehydration is observed around 90°C as the peak at 672 cm^{-1} appears and other peaks
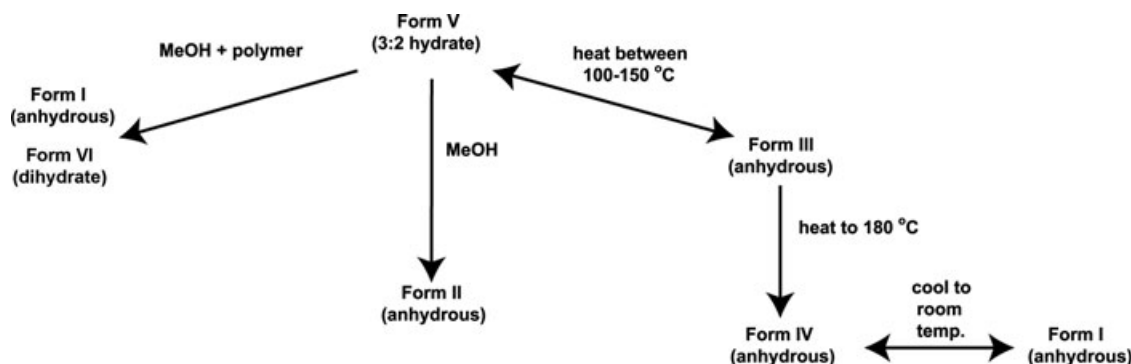

Figure 2.   Schematic representation of observed acyclovir transformations.
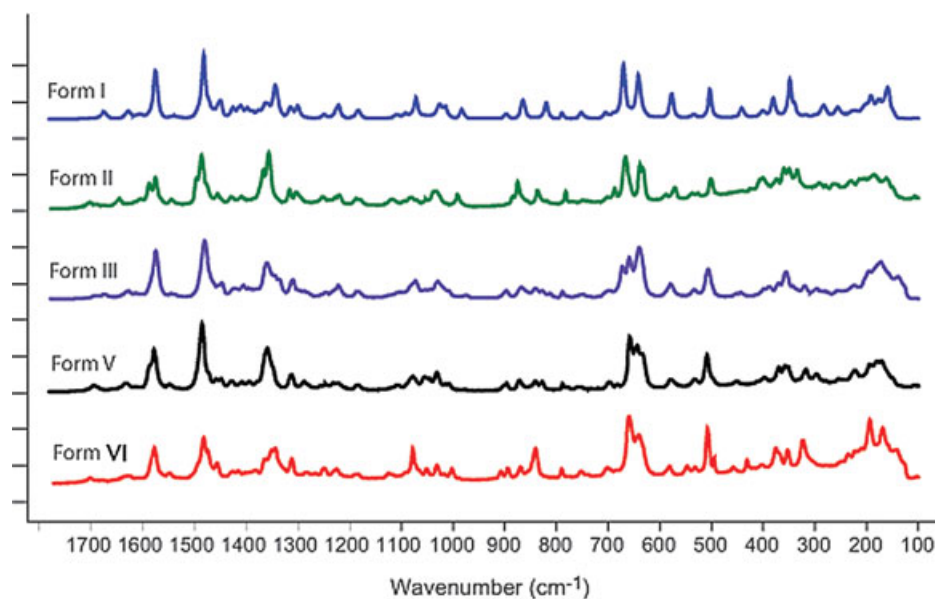
Figure 3. Raman spectra of the five forms of acyclovir (all spectra were taken at room temperature except form III, which was taken at 90°C).

in the spectrum begin to shift. Form III is observed briefly before the transformation to form I. At approximately 180°C, there is another shift observed at 1480 cm^{-1} that is associated with the transition to the high-temperature modification (form IV). Upon cooling to room temperature, form I is observed once again. Figure 5 shows the same transition to the high-temperature modification occurring during the heating of anhydrous form I.

Infrared Spectroscopy

Infrared spectroscopy probes differences in the influence of solid-state form on the molecular level arising from changes in intramolecular and intermolecular interactions.[14,15] Form I, II, and V were sufficiently stable and available in sufficient quantity to allow study by FTIR spectroscopy (Table 2). The main region of difference among the forms is from 1600 to 1200 cm^{-1} (Fig. 6). Forms I and II have very similar FTIR spectra, although the spectra differ mainly in the region around 1700 to 1450 cm^{-1} in which some of the common peaks are shifted to higher or lower wavenumber. These changes can likely be ascribed to alterations of C—C, carbonyl, and C—N stretching frequencies. Another region in which forms I and II have spectral differences is 1300 to 1000 cm^{-1}. In this region, C—O vibrations are often located. These same changes were observed in Raman spectroscopy. Other peaks were shifted in the fingerprint (1000–600 cm^{-1}) region, which can be difficult to assign to specific vibrations by FTIR; nevertheless, Raman spectroscopy is a better technique to analyze differences in this region. Taken together, these data suggest that forms I

and II have some changes in the conformation in the ethoxy chain and the carbonyl region.

From 3600 to 3200 cm^{-1}, the N—H vibration region, forms I and II have very similar spectra (Fig. 6). However, form V has a peak at 3470 cm^{-1} that is not observed in forms I and II. In form V, the carbonyl peak (1750–1640 cm^{-1}) is not well observed compared with forms I and II. The hydrate form V displays some peak shifting in the N—H and C—O regions of the spectra. Because form V is a hydrate, the water molecules in the structure can form more and stronger hydrogen bonds, which lead to shifts of the carbonyl peak to lower wavenumber than in forms I and II. The same pattern was observed by Raman spectroscopy, with some peaks shifted to around 1690 cm^{-1}.

X-ray Diffraction

Powder X-ray diffraction allows reliable differentiation among all ACV forms. Forms I, II, V, and VI were analyzed using PXRD at room temperature, whereas powder patterns of forms III and IV were obtained at high temperature because of the instability of the materials. Distinctive reflections in the powder patterns of the forms include reflections between 2° and 10° 2θ among others. Table 3 lists the reflections observed for all the forms of ACV and Figure 7 shows the powder patterns.

Variable temperature PXRD was also performed on forms I and V. The VT-PXRD of form I (Fig. 8) shows that a high temperature modification appears between 167°C and 170°C. This change corresponds to an endothermic transition observed in DSC (vide infra) and can be associated with a solid–solid transition. VT-PXRD of form V (Fig. 9) shows a total of two

Table 1. Summary of Raman Peak Positions for the Five Forms of Acyclovir

Raman Shift (cm^{-1})	Form I	Form II	Form III	Form V	Form VI
100–200	Three peaks at 159.5, 176.8, and 190.8	Three peaks at 106.0, 162.8, and 185.9	Three peaks at 135.9, 171.1, and 194.8	Two peaks at 179.3 and 193.3	Three peaks at 141.6, 168.6, and 193.2
200–300	Three peaks at 222.15, 255.9, and 283.1	Five peaks at 209.0, 228.7, 258.4, 279.8, and 291.4	Four peaks at 224.3, 255.4, 279.9, and 297.9	Three peaks at 223.0, 254.3, and 296.3	Two peaks at 208.7 and 234.7
300–400	Three peaks at 340.0, 348.2, and 380.3	Four peaks at 334.2, 350.7, 359.7, and 374.57	Five peaks at 320.0, 356.1, 370.0, 388.0, and 398.6	Four peaks at 317.7, 358.1, 369.6, and 397.6	Three peaks at 323.3, 352.8, and 375.7
400–500	Two peaks at 400.9 and 441.3	Two peaks at 400.9 and 425.7	Two peaks at 442.0 and 452.7	One peak at 450.4	Four peaks at 400.3, 431.4, 457.6, and 494.4
500–600	Three peaks at 503.1, 534.4, and 577.3	Five peaks at 500.6, 527.0, 536.9, 571.5, and 588.8	Three peaks at 505.9, 535.3, and 578.7	Three peaks at 508.9, 532.8, and 578.1	Four peaks at 507.5, 531.2, 548.4, and 582.0
600–700	Three peaks at 641.5, 670.4, and 688.5	Four peaks at 632.5, 638.2, 666.2, and 686.8	Three peaks at 639.3, 658.9, and 672.8	Five peaks at 634.1, 644.0, 658.0, 681.9, and 698.4	Three peaks at 640.1, 659.7, and 685.1
700–800	Three peaks at 705.0, 751.9, and 789.0	Five peaks at 700.8, 740.4, 748.6, 770.0, and 782.4	Three peaks at 702.3, 749.0, and 789.1	Three peaks at 756.0, 778.3, and 787.3	Three peaks at 701.5, 753.1, and 789.9
800–900	Three peaks at 819.5, 864.8, and 896.9	Four peaks at 820.3, 836.8, 874.7, and 884.6	Five peaks at 812.8, 826.7, 841.5, 867.7, and 896.3	Four peaks at 827.7, 840.9, 871.4, and 896.1	Three peaks at 840.6, 869.3, and 894.7
900–1000	Two peaks at 932.3 and 983.4	One peak at 990.8	Two peaks at 975.7 and 984.7	One peak at 979.3	One peak at 907.0
1000–1100	Four peaks at 1015.6, 1025.44, 1071.6, and 1092.2	Three peaks at 1036.2, 1052.6, and 1080.6	Two peaks at 1028.1 and 1073.1	Six peaks at 1008.1, 1015.6, 1030.4, 1049.3, 1055.1, and 1078.2	Six peaks at 1001.9, 1016.6, 1031.4, 1051.0, 1078.0, and 1091.1
1100–1200	Two peaks at 1109.5 and 1182.8	Three peaks at 1118.5, 1182.8, and 1187.8	Two peaks at 1104.2 and 1184.5	Two peaks at 1108.7 and 1182.8	Two peaks at 1124.7 and 1185.3
1200–1300	Two peaks at 1221.5 and 1249.5	Two peaks at 1219.9, 1228.9, and 1252.8	Four peaks at 1222.1, 1246.7, 1288.4, and 1298.2	Four peaks at 1221.5, 1232.2, 1247.1, 1257.0, and 1288.3	Four peaks at 1226.2, 1250.0, 1283.5, and 1288.4
1300–1400	Five peaks at 1300.6, 1314.6, 1343.5, 1361.6, 1376.4, and 1397.8	Four peaks at 1303.1, 1316.3, 1356.7, and 1367.4	Three peaks at 1310.5, 1361.26, and 1391.5	Three peaks at 1313.0, 1359.1, and 1394.6	Four peaks at 1312.14, 1344.1, 1351.4, and 1364.5
1400–1500	Five peaks at 1411.0, 1425.9, 1450.6, and 1482.7	Four peaks at 1410.2, 1429.2, 1455.5, and 1486.8	Four peaks at 1405.5, 1421.8, 1447.2, and 1480.8	Five peaks at 1408.6, 1428.3, 1448.9, 1458.8, and 1486.0	Five peaks at 1415.3, 1426.0, 1457.0, 1473.4, and 1482.4
1500–1600	Two peaks at 1540.4 and 1575.8	Three peaks at 1545.3, 1574.8, and 1588.2	Two peaks at 1542.2 ad 1574.9	Two peaks at 1549.4 and 1578.3	Two peaks at 1548.7 and 1578.1
1600–1700	Three peaks at 1606.3, 1628.5, and 1675.5	Three peaks at 1604.6, 1645.8 and 1702.7	Four peaks at 1614.2, 1630.6, 1672.3, and 1692.0	Three peaks at 1614.5, 1631.8, and 1695.3	Three peaks at 1625.7, 1631.4, and 1701.8

transitions upon heating. Form V first dehydrates to produce form III between 65°C and 80°C. Form III then transforms to form IV between 170°C and 180°C. This transition directly correlates to the endotherms observed in the DSC of form V (vide infra). Once the sample was cooled, it had transformed back to form I.

Thermomicroscopy, DSC, and TGA

Thermal studies were performed on ACV using DSC, TGA, and thermomicroscopy. Thermomicroscopy was also combined with Raman spectroscopy to provide additional information about the changes occurring as a function of temperature. TGA showed that forms I and II were anhydrous. Form VI showed a weight loss of 2.9%, whereas form V, the commercial hydrate, showed a weight loss of 5.0%, which is expected of the 3:2 hydrate.

Differential scanning calorimetry was performed on forms I, II, V, and VI (Fig. 10). Form I showed an endothermic transition between 167°C and 176°C and a melt/decomposition centered at 248.8°C with an onset of 245°C. Form II exhibited no transitions prior to a melt/decomposition event centered at 260.1°C (onset of 257.6°C). Form V showed two overlapping transitions between 148°C and 179°C. Form VI exhibited a loss of water between 50°C and 90°C, a transition at 170°C, followed by the melt/decomposition at
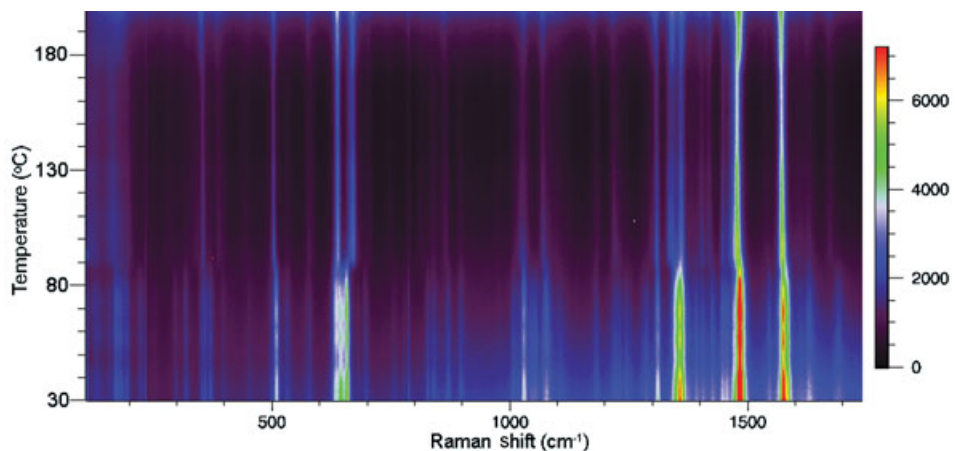
Figure 4. Variable temperature Raman spectroscopy plot starting with form V and showing the Raman shifts during several phase transitions.
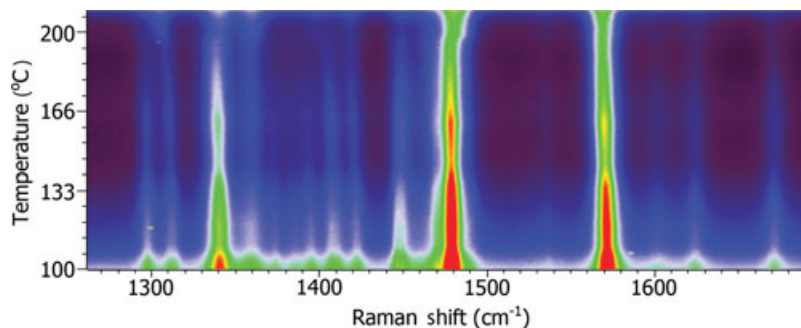

Figure 5. Variable temperature Raman spectroscopy plot starting with form I showing a single-phase transition to form IV.
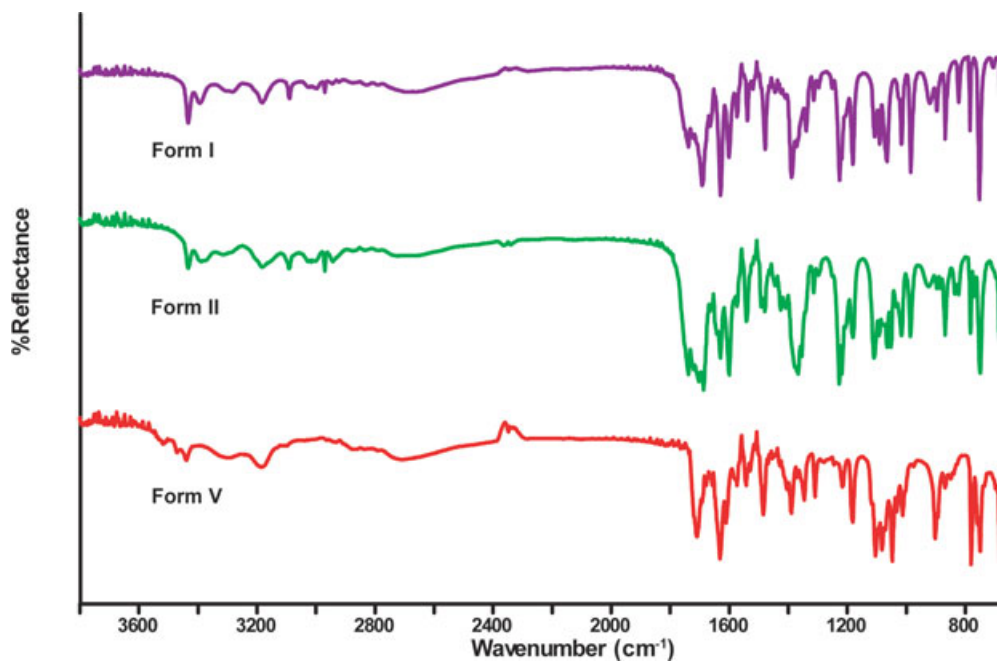

Figure 6. FTIR spectra for forms I, II, and V of acyclovir.

Table 2. Summary of Peak Positions of the FTIR Spectra of Form I, II, and V of Acyclovir

Spectral Range (cm^{-1})	Form I	Form II	Form V
3600–3200	Two peaks at 3432 and 3394	Two peaks at 3433 and 3389	Two peaks at 3470 and 3439
3200–2800	Three peaks at 3182 (broad), 3090, and 2970	Three peaks at 3182 (broad), 3090, and 2970	Single peak at 3182 (broad)
2000–1600	Four peaks at 1737, 1691, 1629 (sharp), and 1600	Five peaks at 1737, 1702, 1686, 1630, and 1600 (sharp)	Three peaks at 1709 (broad), 1631 (sharp), and 1611
1600–1400	Two peaks at 1538 and 1478 (sharp)	Three peaks at 1540, 1492, and 1479	Two peaks at 1542 and 1484 (sharp)
1400–1200	Four peaks at 1388, 1339, 1226, and 1218	Four peaks at 1365 (broad), 1354, 1227, and 1217	Four peaks at 1389, 1345, 1309, and 1215
1200–1000	Five peaks at 1186, 1106, 1090, 1065, and 1016	Six peaks at 1181, 1109, 1091, 1065, 1051, and 1016	Five peaks at 1182, 1104, 1048, 1032, and 1012
1000–800	Four peaks at 985, 920 (broad), 868 (sharp), and 822	Five peaks at 985, 923, 868 (sharp), 835, and 823	Two peaks at 902 and 892
800–600	Three peaks at 783, 752 (sharp), and 680 (sharp)	Four peaks at 782, 770, 749 (sharp), and 682 (sharp)	Four peaks at 780 (sharp), 758, 749, and 682 (sharp)

252.9°C (onset of 250.0°C). Form V showed two over-lapping transitions between 148°C and 179°C and a melt/decomposition of 247.4 (onset of 240.0). When a sample of form I was cycled between 40°C and 190°C repetitively, the same transition was observed during each heating cycle, showing that the transformation is reversible. The DSC thermograms are shown in Figure 10 and the associated data are in Table 4.

Single Crystal X-ray Diffraction

The previously unknown structure of form I was solved from a single crystal grown from a methanol solution in the presence of Nylon 6. In form I, as in all forms of ACV, the guanine ring is planar (Fig. 11)

Table 5. The chain extends above the plane of the guanine ring such that it is in the gauche conforma-tion. The glycosidic torsion angle is 74.3°. Because of the quantity of hydrogen bond donors and accep-tors present in ACV, the hydrogen bonding scheme is extensive (Fig. 12). The amine of the guanine is hy-drogen bonded to the hydroxyl of one molecule at a distance (N···O) of 3.05 Å and the carbonyl of another molecule at a distance (N···O) of 2.92 Å. The hydrogen of the hydroxyl functionality also donates to the car-bonyl. The remaining hydrogen bond is between the secondary nitrogen of the five-membered ring and the N−H of the six-membered ring at a distance (N···N) of 2.82 Å. In total, each ACV molecule participates in
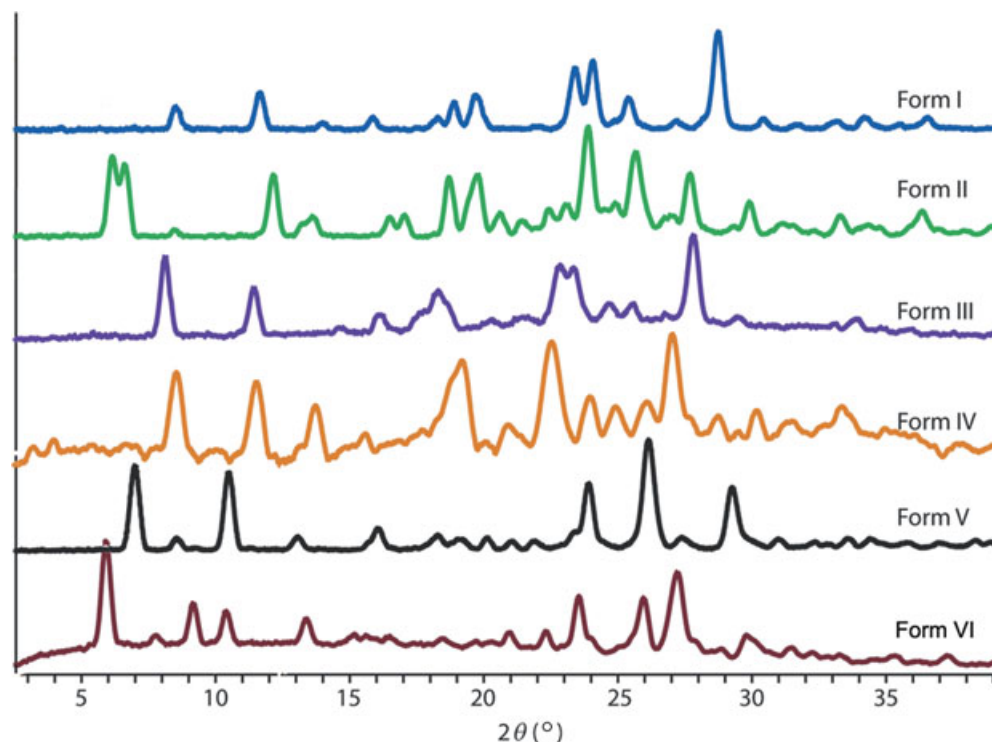

Figure 7. Powder X-ray diffraction patterns of all the forms of acyclovir.

Table 3. Table of Reflections and Intensities for All the Forms of Acyclovir

Form I		Form II		Form III		Form IV		Form V		Form VI	
2θ (°)	Intensity (%)	2θ (°)	Intensity (%)	2θ (°)	Intensity (%)	2θ (°)	Intensity (%)	2θ (°)	Intensity (%)	2θ (°)	Intensity (%)
8.52	21.5	6.23	88.8	8.05	85.5	8.54	53.9	6.99	72.8	5.9	100
11.66	35.6	8.48	6.5	11.35	55.4	11.54	45.1	8.56	8	7.75	6.7
14	6.3	12.14	66.2	12.45	1.8	13.7	23.5	9.26	0.8	9.15	33.7
14.56	0.5	13.55	19.9	13.55	1.5	15.56	6.1	10.5	65.1	10.4	26.3
15.85	11.2	16.56	19.3	14.64	5.5	19.22	63.5	11.34	0.6	13.4	20.2
17.5	1.5	16.99	21.3	16	20.9	20.94	9.2	13.06	8.7	15.19	6.4
18.26	8	18.71	54.2	17.6	21.9	22.54	93.9	16.06	15	15.6	4.6
18.89	21.9	19.72	54.9	18.15	38	23.96	25.3	18.25	7	16.5	3.9
19.72	29.4	20.62	16	18.5	32.3	24.96	16.3	19.1	4.5	17.4	3.8
22.04	2.5	21.43	8.9	19.54	1.2	26.12	15.7	20.13	7.2	18.45	5.2
23.4	55.9	22.48	19.3	20.09	3.9	27.03	100	21.05	5	19.7	2.5
24.07	60.5	23.05	24	21.24	7.4	27.76	2	21.9	4.9	20.25	2.9
25.39	26.7	23.88	100	21.65	3	28.7	8.6	23.42	11.3	20.95	10
27.2	7	24.5	5	22.7	69.1	30.18	16.1	23.92	51.7	22.31	12.2
28.74	100	24.91	7.6	23.25	62	31.18	6.7	26.14	100	23.55	45
30.43	8.9	25.67	83.3	24.5	18.9	31.54	7.2	27.39	6.4	25.95	42.1
31.66	3.9	26.76	8.5	25.45	19.8	32.76	1.9	29.26	48.2	27.2	68
33.17	6.3	26.95	10.4	26.66	2	33.32	16.8	31	5.4	28.85	3.8
34.2	10.3	27.69	64.2	27.7	100	33.76	7.5	32.33	3.2	29.8	15.6
35.48	3.1	29.35	6.3	29.35	8.1	34.91	2.9	32.79	1.6	31.45	5.4
36.53	9.1	29.89	32.5	30.57	1.6	39.98	5.2	33.57	5.2	32.25	2.4
40.09	1.9	31.19	9.2	31.74	1.7			34.45	4.5	32.8	2.9
41.22	4.7	31.5	8.3	33.11	2.6			35.78	2.6	33.25	2.7
42.59	2.5	32.35	2.2	33.7	10.6			36.99	2.8	34.65	1.6
43.72	3.2	33.3	16.9	34.61	2.6			38.32	4	35.35	4.5
45.65	1.6	34.35	7.3	35.7	3.5			38.89	3.1	36.05	2.4
47.89	1.7	34.75	5.9	36.51	1.5			39.97	1.9	37.26	5.8
49.05	2.2	36.35	23.3	39.09	3.4			40.73	3.4	39.2	2.7
		37.94	2.6	40.78	1.1			42.51	1.3	39.75	5.9
		38.94	6.1	41.5	2			43.69	3.6	41.5	5.4
		39.8	7.6	42.75	1.5			44.38	1	42.85	4
		42.1	5.1	43.96	1.4			45.22	1.2	46.45	1.9
		43.96	2.7	46.36	0.7			47.37	1.2	47.3	2
		45.8	3.1	46.97	0.9			48.49	1.6	48.15	2
		46.75	4.7	47.49	1			48.87	2	49.66	0.8
		47.75	3.6	48.39	1.5			49.64	1.3		
		48.6	2.2	48.72	1						
		49.21	3.8								

Table 4. Differential Scanning Calorimetry Data for Forms I, II, V, and VI of Acyclovir

	Form I	Form II	Form V	Form VI
Melt (°C)	248.8	260.1	247.4	252.9
Transition (°C)	165–175	–	150–175	54–70
Transition 2 (°C)	–	–	175–190	70–100
Transition 3 (°C)	–	–	–	165–175
Melt/decomposition (kcal/mol)	8.48	8.24	8.81	6.84
Transition (kcal/mol)	0.57	–	0.44	1.93
Transition 2 (kcal/mol)	–	–	0.06	4.66
Transition 3 (kcal/mol)	–	–	–	0.44

eight hydrogen bonds. The ether and aryl nitrogen do not participate in the hydrogen bonding network. The molecules pack in sheets along the *b*-axis. Along the *c*-axis, the molecules pack in columns such that they alternate the orientation of the guanine ring.

Although a crystal of form II that was of suitable size and quality for single crystal X-ray diffraction was not obtained, a unit cell was determined for a dozen small crystals. The unit cell dimensions are as follows: $a = 4.75$ Å, $b = 15.12$ Å, $c = 28.68$ Å, and $\beta = 91.16°$. Further experimental or theoretical studies will be needed to elucidate the molecular packing pattern and its relation to the other structurally characterized polymorph of ACV.

Acyclovir form VI is a 1:2 ACV/H_2O hydrate with a triclinic unit cell of $a = 6.8004(5)$ Å, $b = 11.3317(9)$ Å, $c = 14.9368(12)$ Å, $\alpha = 82.722(1)°$, $\beta = 82.502(1)°$, and $\gamma = 89.323(1)°$. The side chain of both ACV molecules in the unit cell is in the gauche conformation, whereas the guanine rings are approximately planar. The glycosidic torsion angles are 92.7° and 89.7°. Water molecules are in two channels that run parallel to the *a*-axis. The hydrogen bonding network, such as that of form I, is extensive. In addition to
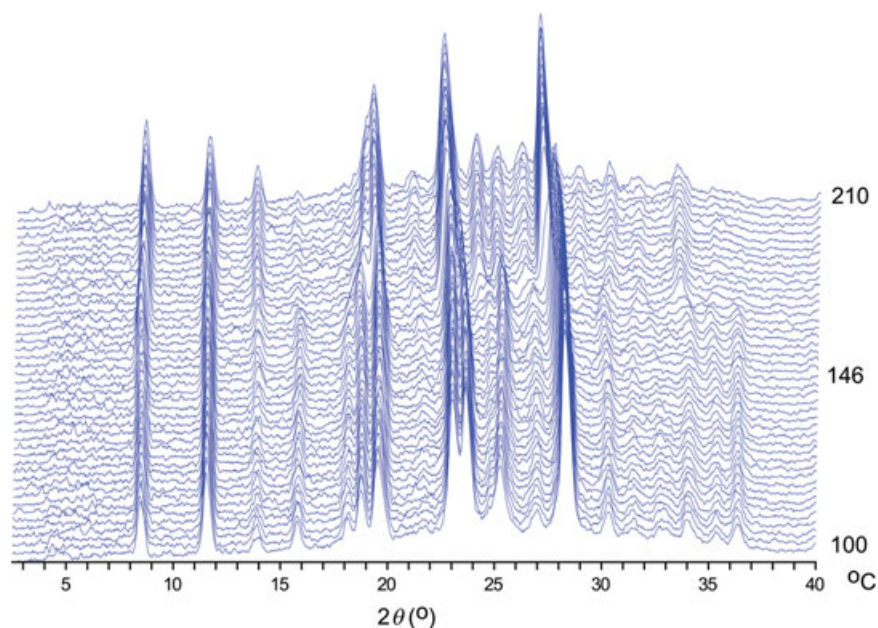
Figure 8. Variable temperature PXRD starting from form I of acyclovir.

hydrogen bonding between ACV molecules, the water molecules are bound not only to each other but also to the ACV molecules surrounding them. The ACV molecules stack such that the chains are orientated toward the water channels and the guanine rings alternate their orientation (Fig. 13).

Form V has two water molecules for every three ACV molecules in the asymmetric unit. The asymmetric unit contains three different ACV molecules. In each molecule, the guanine ring is planar whereas the conformation of the chain varies. In the first residue, the chain is extended almost perpendicular to the plane of the guanine. Its glycosidic torsion angle is

97.2°. Like form I, the chain is in a gauche conformation. The second residue is much like the first, with a glycosidic torsion angle of 104.3°. In the third residue, the chain is fully extended and in the trans conformation. Its glycosidic torsion angle is 91.4°.[6] One water molecule hydrogen bonds to two different molecules of residue 3, one through the carbonyl functionality and the other through the hydroxyl group, in addition to bonding to the hydroxyl group of residue 1. The other water molecule is hydrogen bonded to one molecule of each of the residues; residue 1 hydrogen bonds through the carbonyl, whereas residue 2 hydrogen bonds through a hydroxyl group and
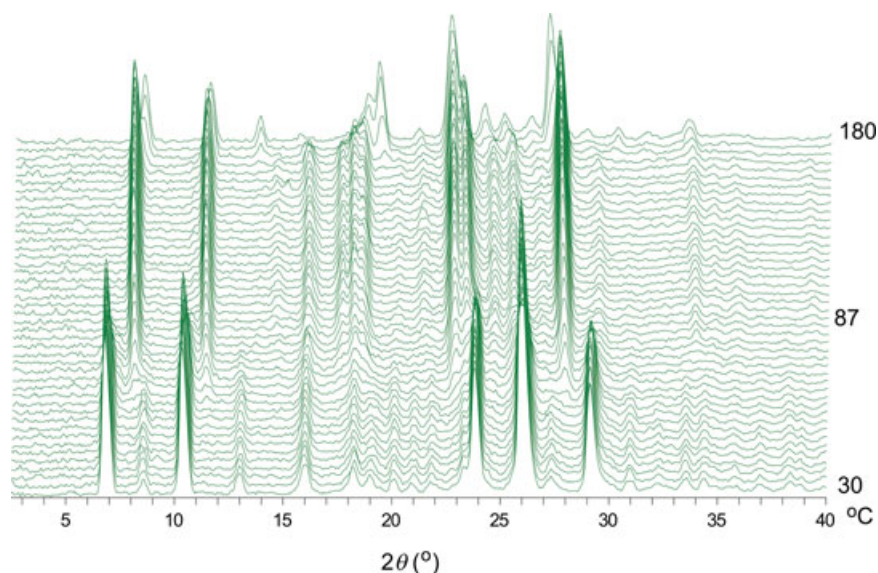

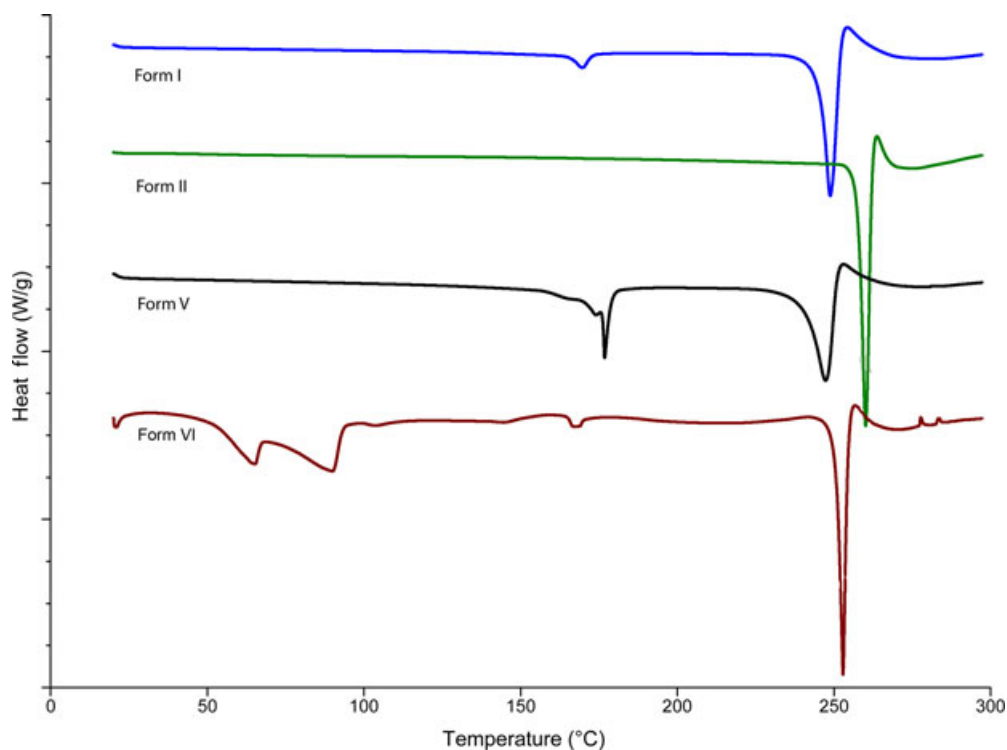**Figure 9.** Variable temperature PXRD starting from form V of acyclovir.

Figure 10. Differential scanning calorimetry thermograms of forms I, II, V, and VI of acyclovir.

residue 3 hydrogen bonds through the amine. The residues themselves form dimers, with residue 1 forming a homodimer and residue 2 dimerizing with residue 3, creating infinite sheets within the crystal structure (Fig. 14).[6]

Solid-State Nuclear Magnetic Resonance

Generally, the most definitive analytical data for polymorph identification is single crystal X-ray diffraction, although for many samples such data are not available. In such cases, solid-state NMR spectroscopy (SS-NMR) can be used to identify the existence of polymorphs and provides detailed information concerning hydrogen bonding interactions.[16,17] Here, SS-NMR was used to further analyze form II because there was no crystallographic informa-

tion for this form. SS-NMR is sensitive to conformational changes and alterations in intermolecular interactions as evidenced by the chemical shifts of the atoms directly involved in the interactions. SS-NMR data were collected at room temperature for forms I, II, and V, revealing significant differences among the forms (Fig. 15). The preliminary assignment of isotropic chemical shifts for ACV forms I and V was made by comparison to computed values (Fig. 1 and Table 6).[12,13] In the low-frequency region, form I has a singlet at 56 ppm whereas form V appears at 61 ppm. Moreover, form II has two peaks detected at 59 and 62 ppm. This low-frequency region is assigned to the ethoxy chain of ACV molecule. There is a 5 ppm upfield shift of C8 resonance from form V compared with form I and 3 ppm compared with form II. This chemical shift difference may be attributed to *gauche* versus
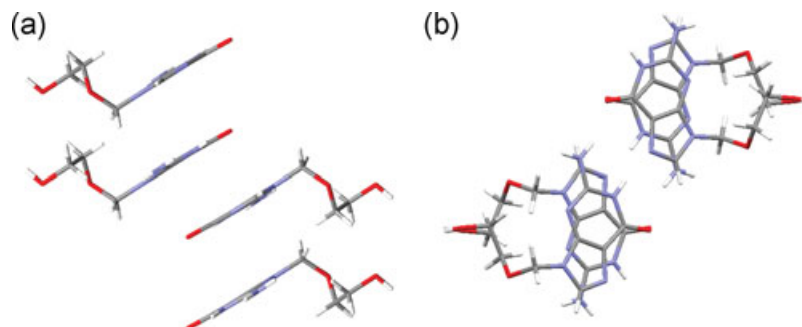

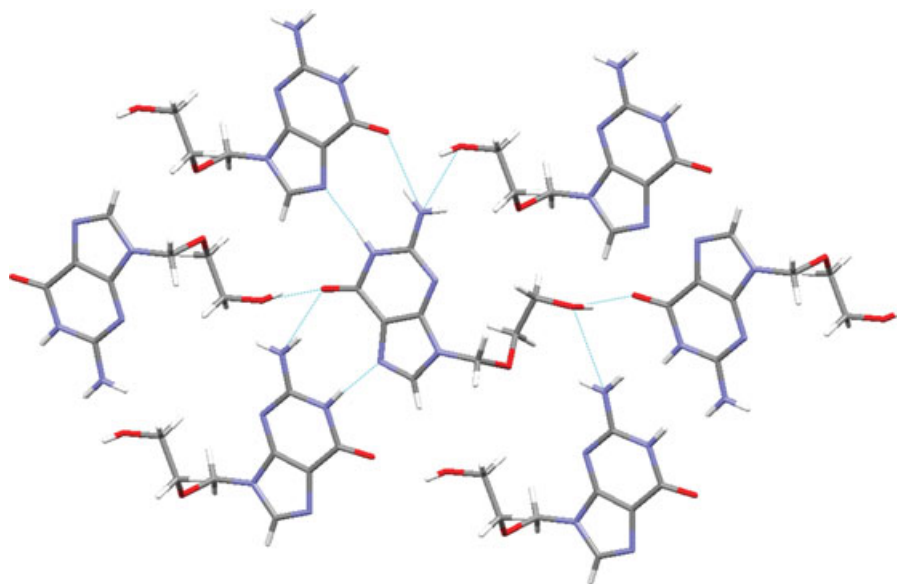**Figure 11.** Packing of form I acyclovir viewed along the (a) *b*-axis and (b) *c*-axis.

Figure 12. Hydrogen bonding interactions present in form I of acyclovir.

trans conformations. In the crystal structure of form I, the chain has adopted a *gauche* conformation. For form V, two of three different ACV molecules have gauche conformation.

In the high-frequency region, a signal at 166 ppm is observed for forms I and II corresponding to the carbonyl carbon (C2). An upfield shift of this peak (to 159 ppm) is observed for form V. This 7-ppm shift can be attributed to the formation of a hydrogen bond to the carbonyl group.[18] Moreover, because form V is a hydrate and forms I and II are not hydrates, this is consistent with expectations from the crystal structure of form V, which has extensive hydrogen bonding compared with form I. The same hydrogen bonding observations and shifts were found from Raman and infrared spectroscopy analyses performed on these forms.

Theoretical NMR calculations of ^{13}C isotropic chemical shifts (Fig. 1 and Table 6) and computed spectra (not shown) reveal very similar shifts compared with the experimental data. However, C8, the carbon at the terminal of the ethoxy chain, in form V

shifts upfield in the experimental data compared with calculations.

Variable Temperature

Further analyses were performed on form V to confirm the existence and the distinctive conversion to form IV at 180°C by variable temperature ^{13}C SS-NMR experiments (Fig. 16). Form V was heated from 30°C to 150°C during MAS inside the probe and no changes were observed in the spectra. However, some differences in the spectra were observed when the temperature of the sample was increased to 180°C consistent with a phase transition to form IV. Peaks observed at 74 and 71 ppm at a low temperature (30°C) were observed as a single peak at 74 ppm when the temperature was increased to 180°C. This can be attributed to rotational/inversion processes that contribute to the site-exchange effect forming a single peak at 180°C.[16,19,20] This process would require the breaking and formation of hydrogen bonds due to the dehydration process. Furthermore, peaks observed at
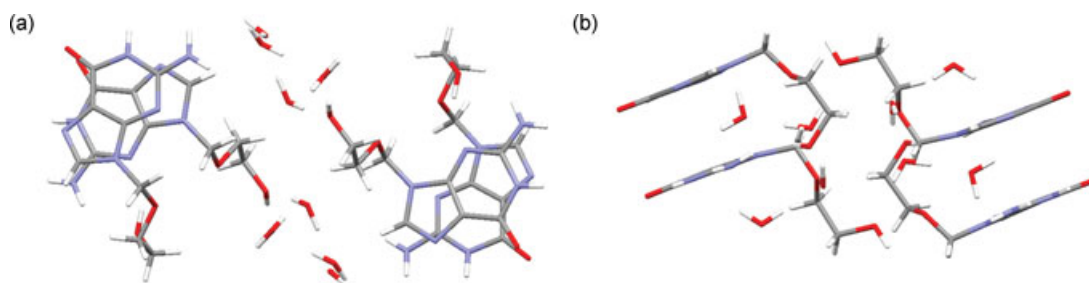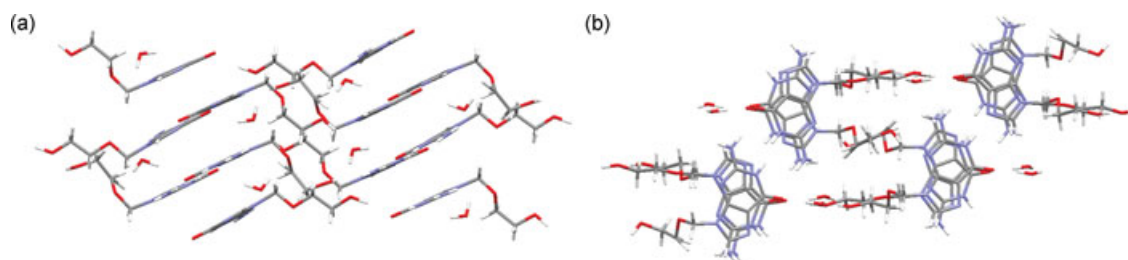

Figure 13. Packing diagram of the 1:2 acyclovir/H_2O down the (a) *a*-axis and (b) *b*-axis.

Table 5. Structural Data of Forms I, V, and VI of Acyclovir and the Hypothetical Unit Cell of Form II

	Form I	Form II	Form V[6]	Form VI
Crystal System	monoclinic	monoclinic	monoclinic	triclinic
Space Group	$P2_1/c$		$P2_1/n$	$P\bar{1}$
Unit Cell				
$a =$	10.9121(11) Å	4.75	25.459(1)	6.8004(5)
$b =$	11.1311(12) Å	15.12	11.282(1)	11.3317(9)
$c =$	7.8843(8) Å	28.68	10.768(1)	14.9368(12)
$\alpha =$	90.00°	90.00°	90.00°	82.722(1)
$\beta =$	108.262(2)°	91.16°	95.16(1)	82.502(1)
$\gamma =$	90.00°	90.00°	90.00°	89.323(1)
Volume	909.422		3080.34	1131.98
Z	4		12	4
Density	1.645 g/cm³		1.63 g/cm³	1.533 g/cm³
Crystal Size	0.11 × 0.03 × 0.01		0.550 × 0.125 × 0.025	0.22 × 0.10 × 0.02
Goodness of Fit	1.051			1.031
Final R indices (obs data) [I> 2σ(I)]	0.0427			0.0365
Final R indices (all data)	0.0652			0.0523
wR	0.0886			0.0857

Figure 14. Packing diagram of the commercial hydrate viewed along the (a) *b*-axis and (b) *c*-axis.
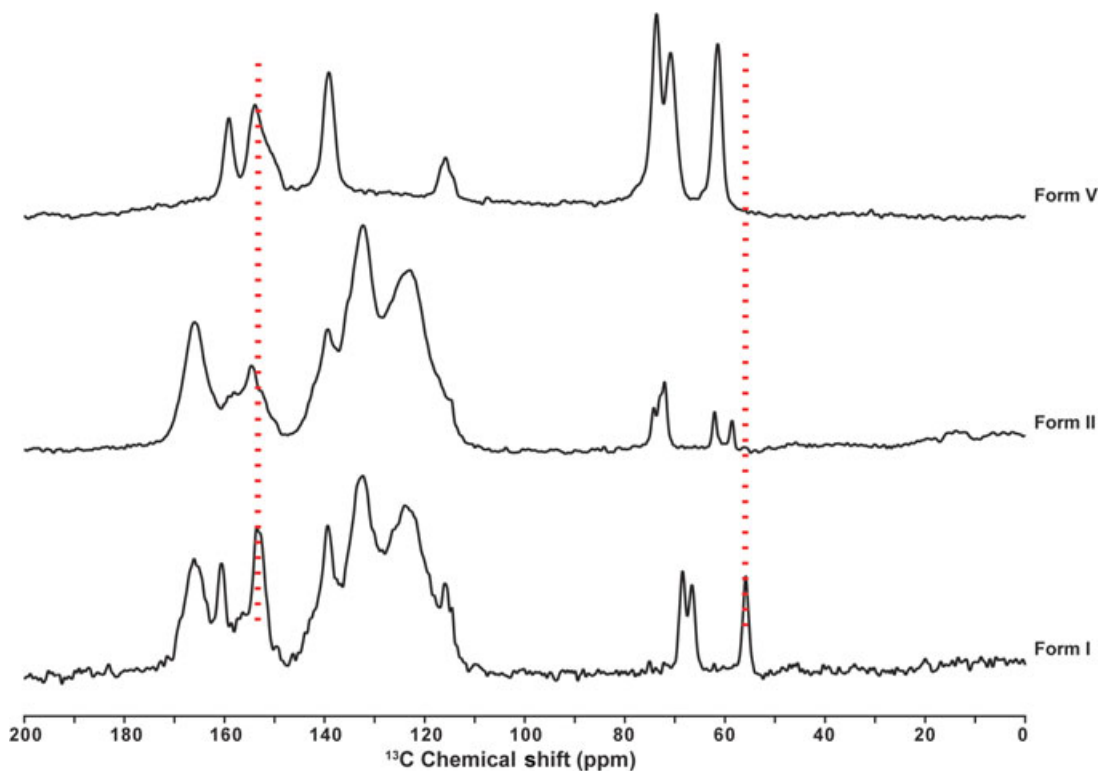
Figure 15. Cross-polarization magic angle spinning ¹³C NMR spectra of forms I, II, and V of acyclovir at ambient temperature.
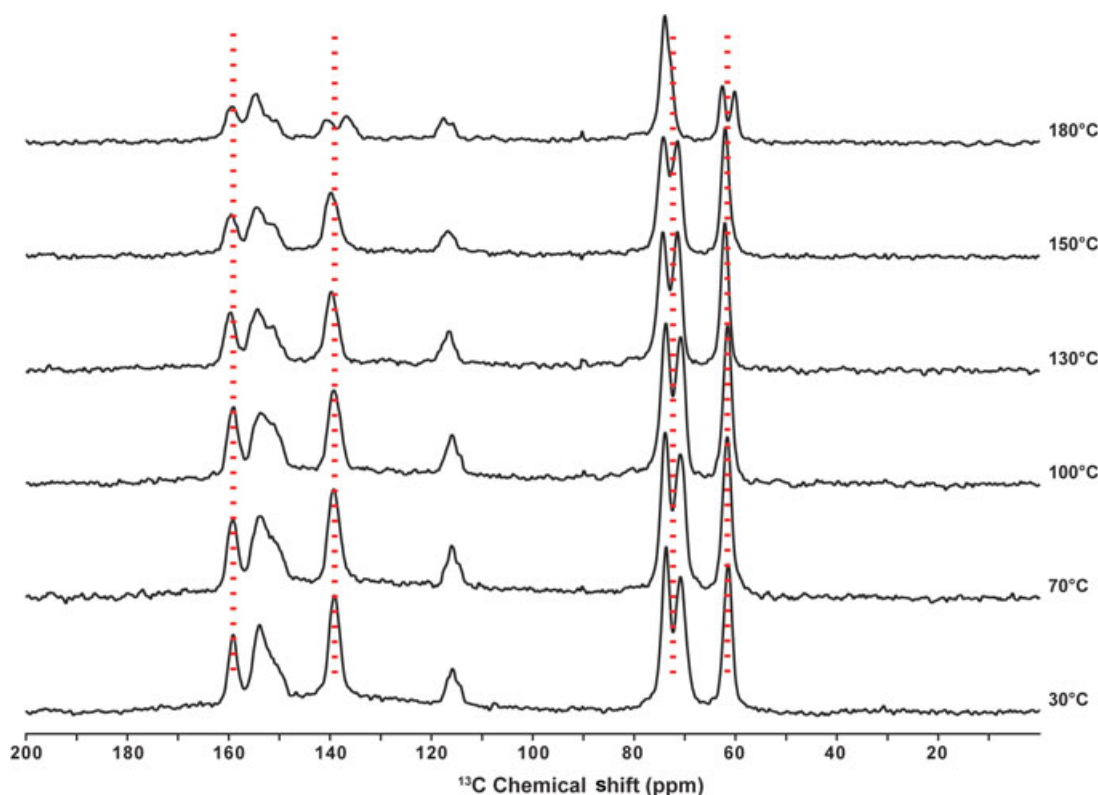
Figure 16. Variable temperature cross-polarization magic angle spinning ^{13}C NMR spectra of acyclovir form V heated from 30°C to 180°C.

Table 6. ^{13}C Chemical Shifts (ppm) Using the GIAO Method and B3LYP Hybrid Functional and 6-311++G (2d,p) Basis Set for Acyclovir Forms I and V

	^{13}C Chemical Shift (ppm)							
	C1	C2	C3	C4	C5	C6	C7	C8
Form I	155.3	161.0	123.6	154.2	141.4	69.4	71.7	62.6
Form V	153.1	161.3	125.1	154.3	140.1	76.1	75.3	66.5
	153.1	161.0	127.1	149.9	140.8	78.3	71.9	65.3
	156.7	158.5	126.3	154.7	137.8	76.1	73.1	62.4

62 and 139 ppm at a low temperature were observed as two peaks at 63 and 60 ppm and 141 and 137 ppm, respectively, at 180°C. From the observed chemical shifts and intensities of the peaks, it can be concluded that form V undergoes a phase transition at 180°C to form IV. ^{13}C chemical shifts are strongly influenced by torsion angles of molecules and at high temperatures the molecules have more mobility than at low temperature. This observation is consistent with the variable temperature Raman data (Fig. 4), in which a change in 1480 cm^{-1} can be correlated to -CH$_2$ bending located in the ethoxy chain of ACV. Moreover, at this temperature, the form V is dehydrated apparently to a phase with more motion. When the sample is cooled from 180°C to 30°C, no major changes were observed in the SS-NMR spectra consistent with the inability of the material to rehydrate or further transform under these conditions (Fig. 17).

CONCLUSION

Using a range of techniques, we have conclusively shown that ACV has several forms ranging from hydrates to anhydrates. Raman spectra and PXRD patterns are reported for all six forms. The crystal structures of the anhydrous form I and both hydrate forms (form V and form VI) have been determined. Although the unit cell of the anhydrous form II was determined, the crystal structure remains elusive. The existence under nonambient conditions of forms III and IV was also shown through PXRD. The anhydrate form IV was found using variable temperature analysis as a transformation from commercial hydrate form V for the first time. Solid-state NMR provided direct chemical information on the forms and allowed following the phase transformation *in situ*. However, the precise mechanism of the phase transformation in terms of the dehydration process has not yet been elucidated. Significant differences in intermolecular hydrogen bonding networks were observed among the ACV forms and are consistent with the solid-state NMR and vibrational spectroscopy analysis exhibiting distinct chemical shifts and vibrational frequencies.
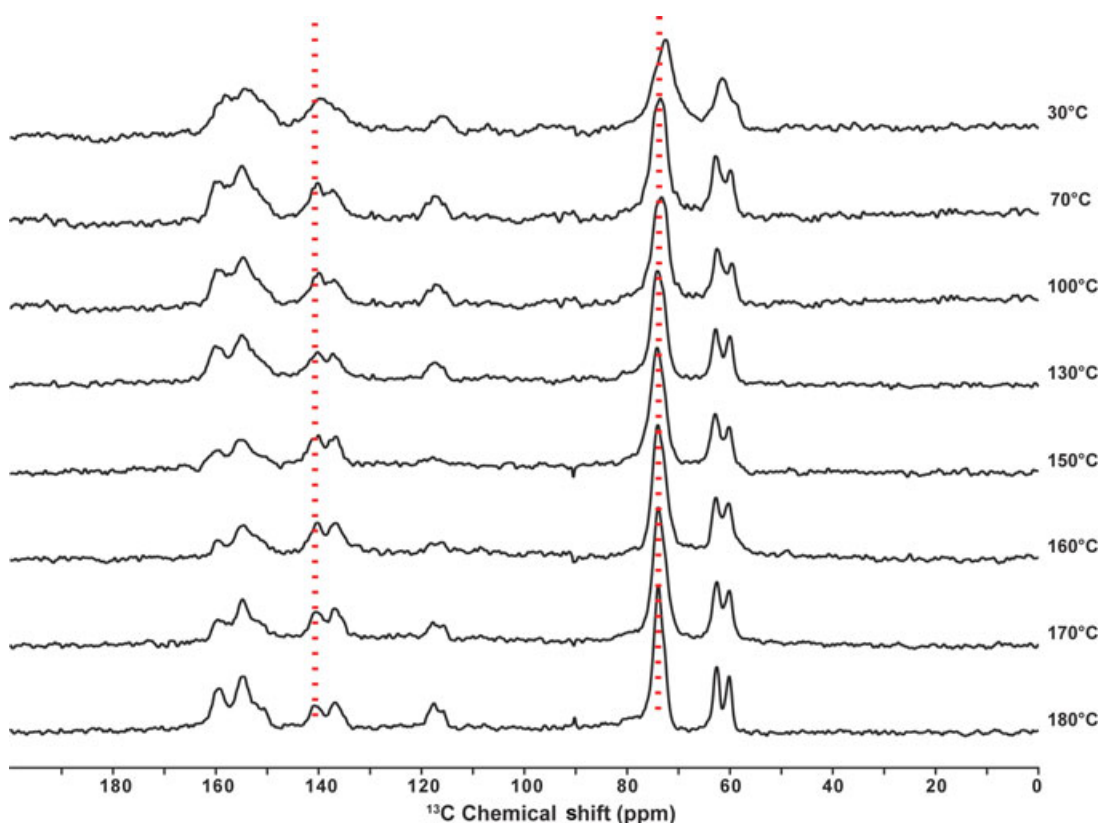
Figure 17. Variable temperature cross-polarization magic angle spinning ^{13}C NMR spectra of acyclovir form V upon cooling.

ACKNOWLEDGMENTS

REFERENCES

1. Brittain HG. 1999. Polymorphism in pharmaceutical solids. New York: Marcel Dekker.
2. Yu L, Reutzel-Edens SM, Mitchell CA. 2000. Crystallization and polymorphism of conformationally flexible molecules: Problems, patterns, and strategies. Org Process Res Dev 4(5):396–402
3. Lang MD, Grzesiak AL, Matzger AJ. 2002. The use of polymer heteronuclei for crystalline polymorph selection. J Am Chem Soc 124(50):14834–14835.
4. Price CP, Grzesiak AL, Matzger AJ. 2005. Crystalline polymorph selection and discovery with polymer heteronuclei. J Am Chem Soc 127(15):5512–5517.
5. Birnbaum GI, Cygler M, Kusmierek JT, Shugar D. 1981. Structure and conformation of the potent anti-herpes agent 9-(2-hydroxyethoxymethyl)guanine (acycloguanosine). Biochem Biophys Res Commun 103(3):968–974.
6. Birnbaum GI, Cygler M, Shugar D. 1984. Conformational features of acyclonucleosides—structure of acyclovir, an anti-herpes agent. Can J Chem 62(12):2646–2652.
7. Kristl A, Srcic S, Vrecer F, Sustar B, Vojnovic D. 1996. Polymorphism and pseudopolymorphism: Influencing the dissolution properties of the guanine derivative acyclovir. Int J Pharm 139(1–2):231–235.

8. Sohn YT, Kim SH. 2008. Polymorphism and pseudopolymorphism of acyclovir. Arch of Pharm Res 31(2):231–234.
9. Shefter E, Higuchi T. 1963. Dissolution Behavior of Crystalline Solvated and nonsolvated forms of some pharmaceuticals. J Pharm Sci 52:781–791.
10. Metz G, Wu X, Smith SO. 1994. Ramped-amplitude cross polarization in magic-angle-spinning NMR. J Magn Reson A 110(2):219–227.
11. Bennett AE, Rienstra CM, Auger M, Lakshmi KV, Griffin RG. 1995. Heteronuclear decoupling in rotating solids. J Chem Phys 103(16):6951–6958.
12. Birn J, Poon A, Mao Y, Ramamoorthy A. 2004. Ab initio study of 13Cα chemical shift anisotropy tensors in peptides. J Am Chem Soc 126(27):8529–8534.
13. Brender JR, Taylor DM, Ramamoorthy A. 2001. Orientation of amide-nitrogen-15 chemical shift tensors in peptides: A quantum chemical study. J Am Chem Soc 123(5):914–922.
14. McGuire GE, Weiss PS, Kushmerick JG, Johnson JA, Simko SJ, Nemanich RJ. 1997. Surface characterization. Anal Chem 69:231R-250R.
15. Threlfall TL. 1995. Analysis of organic polymorphs: A review. Analyst 120:2435–2459.
16. Harris RK. 2006. NMR studies of organic polymorphs & solvates. Analyst 131(3):351–373.
17. Harris RK. 2007. Applications of solid-state NMR to pharmaceutical polymorphism and related matters. J Pharm Pharmacol 59(2):225–239.
18. Gobetto R, Nervi C, Valfre E, Chierotti MR, Braga D, Maini L, Grepioni F, Harris RK, Ghi PY. 2005. H-1 MAS, N-15 CPMAS, and DFT investigation of hydrogen-bonded supramolecular adducts between the diamine 1,4-diazabicyclo-[2.2.2]octane and dicarboxylic acids of variable chain length. Chem Mater 17(6):1457–1466.

19. Rubin-Preminger JM, Bernstein J, Harris RK, Evans IR, Ghi PY. 2004. Variable temperature studies of a polymorphic system comprising two pairs of enantiotropically related forms: [*S*,*S*]-ethambutol dihydrochloride. Cryst Growth Des 4(3):431–439.

20. Stephenson GA, Stowell JG, Toma PH, Dorman DE, Greene JR, Byrn SR. 1994. Solid-state analysis of polymorphic, isomorphic, and solvated forms of dirithromycin. J Am Chem Soc 116(13):5766–5773.